

THE FLATTENED DARK MATTER HALO OF M31 AS DEDUCED FROM THE OBSERVED H I SCALE HEIGHTS

ARUNIMA BANERJEE AND CHANDA J. JOG

Department of Physics, Indian Institute of Science, Bangalore 560012, India; arunima_banerjee@physics.iisc.ernet.in,
cjjog@physics.iisc.ernet.in

Received 2008 April 4; accepted 2008 June 4

ABSTRACT

In this paper we use the outer galactic H I scale height data as well as the observed rotation curve as constraints to determine the halo density distribution of the Andromeda galaxy (M31). We model the galaxy as a gravitationally coupled system of stars and gas, responding to the external force field of a known Hernquist bulge and the dark matter halo, the density profile of the latter being characterized by four free parameters. The parameter space of the halo is optimized so as to match the observed H I thickness distribution as well as the rotation curve on an equal footing, unlike the previous studies of M31 which were based on rotation curves alone. We show that an oblate halo, with an isothermal density profile, provides the best fit to the observed data. This gives a central density of $0.011 M_{\odot} \text{ pc}^{-3}$, a core radius of 21 kpc, and an axis ratio of 0.4. The main result from this work is the flattened dark matter halo for M31, which is required to match the outer galactic H I scale height data. Interestingly, such flattened halos lie at the most oblate end of the distribution of halo shapes found in recent cosmological simulations.

Subject headings: galaxies: halos — galaxies: ISM — galaxies: kinematics and dynamics — galaxies: spiral — galaxies: structure

1. INTRODUCTION

It is well known that the dark matter halo plays an important role in the dynamics of galaxies, especially in the outer regions (Binney & Tremaine 1987). Since a galactic disk is rotationally supported, the rotation curve serves as a useful tracer of the gravitational potential in the plane of the galaxy. The observed rotation curve is routinely used to deduce the mass distribution in a galaxy and, hence, its dark matter content (e.g., Begeman 1987; Kent 1986, 1987; Geehan et al. 2006). The thickness of the gas layer, on the other hand, depends on the vertical gravitational force and traces the potential perpendicular to the midplane (e.g., Narayan & Jog 2002a). In this work we use the rotation curve as well as the radial distribution of the thickness of the H I gas layer in the outer galaxy to study the shape and density profile of the dark matter halo in M31. In a disk plus bulge plus halo model of an external galaxy, the disk and the bulge can be mostly studied observationally. Therefore, the rotation curve and the vertical H I scale height data effectively complement each other to determine the dark matter halo distribution of a galaxy uniquely.

In the past, the idea of studying the dark matter halo properties by using the outer galactic H I flaring data has been used to explore the halos of NGC 4244 (Olling 1996), NGC 891 (Becquaert & Combes 1997), and the Galaxy (Olling & Merrifield 2000, 2001). However, the H I scale height distribution was mainly used to constrain the oblateness of the halo and not its other parameters such as the power-law index. In some cases, the gas gravity and even the stellar gravity were ignored (Becquaert & Combes 1997) in determining the net galactic potential and, hence, the gas scale height distribution.

These issues were taken care of in determining the Galactic halo parameters by Narayan et al. (2005). Using the gravitationally coupled, three-component Galactic disk model (Narayan & Jog 2002b), various density profiles of the halo were investigated, and an attempt was made to obtain the halo parameters, which provided the best fit (in the least-square sense) to the observed H I scale height distribution. Finally, conformity with the shape of the observed rotation curve was used to remove the degen-

eracies in the best-fit values obtained by the first constraint. Also, unlike some of the previous models, the self-gravity of the gas was included in the analysis. From their study, Narayan et al. (2005) concluded that a spherical halo, with a density falling off more rapidly than an isothermal halo, provides the best fit to the available data. This study was based on the H I scale height data then available up to 24 kpc from Wouterloot et al. (1990). Kalberla et al. (2007) have confirmed this by using their recent extended H I scale height data up to 40 kpc and have also included a dark matter ring which they claim is needed to explain the observed H I scale height distribution in the Galaxy.

In this paper we apply the above approach to investigate the dark matter halo properties of the Andromeda galaxy (M31 or NGC 224). Here we use both the rotation curve and the H I scale height data as rigorous constraints simultaneously and scan the entire parameter space systematically so as to obtain the best-fit halo parameters. In addition to the various density profiles, we also try to fit various shapes of the halo, which was not done by Narayan et al. (2005). Earlier studies on M31 (Widrow et al. 2003; Widrow & Dubinski 2005; Geehan et al. 2006; Seigar et al. 2008; Tamm et al. 2007) were mostly aimed at developing a complete mass model (disk plus bulge plus halo), based on comparisons made with the available structural and kinematical data (surface brightness profiles, bulge-velocity dispersion relations, rotation curves), which assumed a spherical-shaped halo. On the other hand, we have studied the dark matter halo profile and show it to be flattened.

In § 2 we describe our model and, in § 3, discuss the numerical calculations involved and the input parameters used. In § 4 we present the results and analysis of the numerical results, followed by the discussion and conclusions in §§ 5 and 6, respectively.

2. DETAILS OF THE MODEL

2.1. *Gravitationally Coupled, Three-Component, Galactic Disk Model*

A galaxy is modeled as a thick stellar disk, coplanar with the interstellar medium of atomic and molecular hydrogen gas, all three components being gravitationally coupled to each other

and embedded in the dark matter halo (Narayan & Jog 2002b). The bulge and the dark matter halo are taken to be rigid and non-responsive, and act as external forces on the three-component disk system. Also, it is assumed that the components are in hydrostatic equilibrium in the vertical direction. Therefore, the density distribution of each component will be jointly determined by the Poisson equation and the corresponding equation for pressure equilibrium perpendicular to the midplane.

The Poisson equation for an axisymmetric galactic system in terms of the galactic cylindrical coordinates (R, ϕ, z) is given by

$$\frac{\partial^2 \Phi_{\text{tot}}}{\partial z^2} + \frac{1}{R} \frac{\partial}{\partial R} \left(R \frac{\partial \Phi_{\text{tot}}}{\partial R} \right) = 4\pi G \left(\sum_{i=1}^3 \rho_i + \rho_b + \rho_h \right), \quad (1)$$

where ρ_i with $i = 1-3$ denotes the mass density for each disk component, ρ_h and ρ_b denote the same for the halo and the bulge, respectively, and Φ_{tot} denotes the net potential due to the disk, halo, and the bulge. For a flat or gently falling rotation curve, the radial term can be neglected, as its contribution to the determination of the H I scale height is less than 10% as noted by earlier calculations (Narayan et al. 2005). So, the above equation reduces to

$$\frac{\partial^2 \Phi_{\text{tot}}}{\partial z^2} = 4\pi G \left(\sum_{i=1}^3 \rho_i + \rho_b + \rho_h \right). \quad (2)$$

The equation for hydrostatic equilibrium in the z -direction is given by (Rohlfs 1977)

$$\frac{\partial}{\partial z} \left[\rho_i \langle (v_z^2)_i \rangle \right] + \rho_i \frac{\partial \Phi_{\text{tot}}}{\partial z} = 0, \quad (3)$$

where $\langle (v_z^2)_i \rangle$ is the mean square random velocity along the z -direction for the component i . We further assume each component to be isothermal for simplicity, so that the velocity term is constant with z .

Eliminating Φ_{tot} between equation (2) and equation (3) and assuming an isothermal case, we get

$$\langle (v_z^2)_i \rangle \frac{\partial}{\partial z} \left(\frac{1}{\rho_i} \frac{\partial \rho_i}{\partial z} \right) = -4\pi G \left(\sum_{i=1}^3 \rho_i + \rho_b + \rho_h \right), \quad (4)$$

which represents a set of three coupled, second-order differential equations, one for each component of the disk. From the above equation, it is evident that although there is a common gravitational potential, the response of each component will be different due to the difference in their random velocity dispersions.

2.2. Bulge

We model the bulge of M31 as a spherically symmetric mass distribution represented by a Hernquist profile (Hernquist 1990), where M_b is the total mass of the bulge and r_b is its core radius. The mass profile and density corresponding to this distribution are given by

$$M_{\text{bul}}(R) = \frac{M_b R^2}{(r_b + R)^2}, \quad (5)$$

$$\rho_{\text{bul}}(R) = \left(\frac{M_b}{2\pi r_b^3} \right) \frac{1}{(R/r_b)(1 + R/r_b)^3}, \quad (6)$$

respectively. Since M31 is an Sb type galaxy, the bulge contribution is important and plays a role in determining the rotation curve even in regions outside the bulge.

2.3. Dark Matter Halo

We use the four-parameter dark matter halo model (de Zeeuw & Pfenniger 1988; Becquaert & Combes 1997) with the density profile given by

$$\rho(R, z) = \frac{\rho_0}{[1 + m^2/R_c^2]^p}, \quad (7)$$

where $m^2 = R^2 + (z^2/q^2)$, ρ_0 is the central core density of the halo, R_c is the core radius, p is the density index, and q is the vertical-to-planar axis ratio of the halo (spherical: $q = 1$; oblate: $q < 1$; prolate: $q > 1$).

3. NUMERICAL CALCULATIONS

3.1. Solution of Equations

For a given bulge and halo density profile, the equation to be solved to obtain the vertical density distribution at any radius for any component (stars, H I, and H₂) is given by equation (4), which simplifies to

$$\frac{d^2 \rho_i}{dz^2} = \frac{\rho_i}{\langle (v_z^2)_i \rangle} [-4\pi G(\rho_s + \rho_{\text{H1}} + \rho_{\text{H2}} + \rho_b + \rho_h)] + \frac{1}{\rho_i} \left(\frac{d\rho_i}{dz} \right)^2. \quad (8)$$

This represents three coupled, second-order, ordinary differential equations in ρ_s , ρ_{H1} , and ρ_{H2} which denote the mass densities for stars, H I, and H₂, respectively. This problem is solved in an iterative fashion, as an initial value problem, using a fourth-order, Runge-Kutta method of integration, with the following two initial conditions at the midplane, i.e., $z = 0$ for each component,

$$\rho_i = (\rho_0)_i, \quad \frac{d\rho_i}{dz} = 0. \quad (9)$$

However, the modified midplane density $(\rho_0)_i$ for each component is not known a priori. Instead, the net surface density $\Sigma_i(R)$, given by twice the area under the curve of $\rho_i(z)$ versus z , is used as the second boundary condition, since this is known observationally. Hence, the required value of $(\rho_i)_0$ can be determined by trial and error, which eventually fixes the $\rho_i(z)$ distribution. We find that four iterations are adequate to give convergence with an accuracy to the second decimal place. For a three-component disk, the vertical distribution is steeper than a sech² distribution close to the midplane (Banerjee & Jog 2007), but at large- z values, it is close to a sech² distribution. Here we use the half-width at half-maximum of the resulting model vertical distribution to define the scale height as was done in Narayan & Jog (2002a, 2002b).

3.2. Input Parameters for M31

The model described so far is general; now we apply it to M31. For that, we require the surface density and the vertical velocity dispersion for each component to solve the coupled set of equations at each radius. The observed values are used for the gas, whereas for the bulge and the stellar component the values derived from the mass model are used except for the vertical dispersion velocity of the stars.

The radial distribution of the H I surface density is taken from Sofue & Kato (1981), while the surface density for the H₂ gas, being an order of magnitude smaller and confined to the inner region (Koper 1993), was taken to be zero. The vertical dispersion velocity of the H I gas, $(v_z)_{\text{H}\text{I}}$, is taken to be 8 km s⁻¹, as given by the observations of a large sample of about 200 external galaxies (Lewis 1984).

For the stars, we assume an exponential disk with a central surface density of $460 M_{\odot} \text{ pc}^{-2}$ and an exponential disk scale length R_d of 5.4 kpc, after Geehan et al. (2006). The disk scale length matches with the *R*-band scale length of Widrow et al. (2003), whereas Koper (1993) gives a value of 5.1 kpc. Also, the maximum disk mass of $8 \times 10^{10} M_{\odot}$ predicted by the Widrow et al. (2003) model sets the central disk surface density value to $440 M_{\odot} \text{ pc}^{-2}$ for $R_d = 5.4$ kpc. So the difference between the values used in our work with other values in the literature is of the order of a few percent.

The bulge is taken to have a Hernquist profile as described above, with a total mass M_b of $3.3 \times 10^{10} M_{\odot}$ and a core radius r_b of 0.61 kpc, as given by the same model (Geehan et al. 2006). Kerins et al. (2001) give a mass M_b of $4 \times 10^{10} M_{\odot}$, whereas Widrow et al. (2003) give a mass of $2.5 \times 10^{10} M_{\odot}$. As expected, the bulge becomes progressively less important as we move radially outward in the galaxy, and so is not important in the determination of the rotation curve or the H I scale height in the outer parts, which is our region of interest. However, it does affect the determination of the rotation curve in the intermediate range; hence, the bulge has to be included for a correct treatment of the problem.

The stellar radial velocity dispersion is assumed to fall off exponentially with a scale length of $2R_d$, as is observed in the Galaxy (Lewis & Freeman 1989); for M31, this gives a value of 10.8 kpc. Also, the ratio of the vertical to the radial stellar velocity dispersion is taken to be 0.5 at all radii, equal to its observed value in the solar neighborhood (Binney & Merrifield 1998). Based on these, the central value of 126 km s⁻¹ for the radial dispersion is deduced from the observed value at $2R_d$ for M31 by Tamm et al. (2007).

4. RESULTS AND ANALYSIS

4.1. Halo Density Profiles: The Three-dimensional Grid

We scan the allowed values for the entire parameter space for the dark matter halo, to obtain the best fits to the data for the rotation curve and the H I scale heights in the outer parts of M31. We vary the halo density index p between 1, 1.5, and 2. Here $p = 1$ corresponds to the isothermal and $p = 1.5$ to the NFW (Navarro et al. 1996) halo density profile at large radii. These two profiles are routinely used in galactic mass modeling and other studies. Narayan et al. (2005) found that a steeper than NFW profile ($p = 2$) best conforms with the H I scale height data in the outer regions of our Galaxy, suggesting evidence of finite-sized halos. So, we study each of the above three cases individually. For each value of p , a realistic range of ρ_0 and R_c for the spherical case is chosen to form a grid of (ρ_0, R_c) pairs. The central core density of the halo ρ_0 is varied between 0.001 and $0.15 M_{\odot} \text{ pc}^{-3}$ in steps of $0.002 M_{\odot} \text{ pc}^{-3}$, and R_c is varied between 1 and 35 kpc in steps of 0.5 kpc. At first, we use a spherical halo for simplicity. Although it gives the correct rotation curve, it fails to match the outer galactic H I scale height data within the error bars. Figure 1 shows that the outer galactic H I scale height distribution obtained by using the best-fit values for a spherical isothermal halo ($p = 1$) flares far above the observed data, giv-

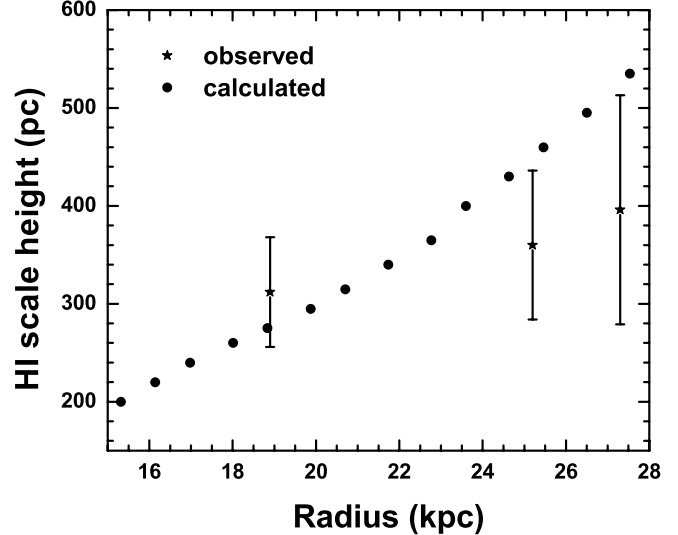


FIG. 1.—Plot of the H I scale height (in pc) with the galactocentric radius (in kpc) for the best-fit case for the spherical shape ($q = 1$) halo for the density law $p = 1$ (isothermal). Clearly, the model curve rises way above the observed distribution in the outer galaxy which is the region of interest. Thus, a spherical halo is ruled out.

ing a poor fit. The same is found to be true for the other density profiles ($p = 1.5$ and 2) as well.

This naturally called for the use of an oblate (flattened) halo, because the midplane surface density increases with the flattening of the halo, thus resulting in a higher vertical constraining force. The effect, as expected, is exactly the opposite of the case of a prolate halo. The latter would therefore give an even poorer fit than the spherical case and, hence, is not tried here. Therefore, in addition to the above parameters, the axis ratio q is varied as well between 0.1 and 0.9 in steps of 0.1. This gives a total of 47,250 grid points to be scanned for each value of p . We first thoroughly scan this grid to locate the region of minimum χ^2 .

In retrospect, Narayan et al. (2005) had pinned the rotation curve at a single point only (i.e., the solar point with $R = 8.5$ kpc) using the local Oort constants A and B , for which the values are available for the Galaxy. This effectively fixed the rotation curve locally, with respect to the shape as well. Also, the global trends exhibited by the observed curve were used as the final criterion to choose the best-fit density index ($p = 2$). Here, on the other hand, we apply a more rigorous treatment by pinning the rotation curve at all the observed points. This, in fact, was imperative since the Oort A and B constants for M31 are not known.

4.2. The Rotation Curve Constraint

For each of the above grid points, we evaluate the galactic rotation curve using our (disk plus bulge plus halo) model as follows. For an exponential disk, the rotation velocity $v_{\text{disk}}(R)$ is given by (Binney & Tremaine 1987)

$$v_{\text{disk}}^2(R) = 4\pi G \Sigma_0 R_d y^2 [I_0(y)K_0(y) - I_1(y)K_1(y)], \quad (10)$$

where Σ_0 is the disk central surface density, R_d the disk scale length, $y = R/2R_d$, R being the galactocentric radius, and I_n and K_n (where $n = 0$ and 1) are the modified Bessel functions of the first and second kinds, respectively. The above relation is for an infinitesimally thin disk which we use here for simplicity. For a thick disk, a separate result has to be used (as given in Becquaert & Combes 1997), which we check gives a value within $< 1\%$ of

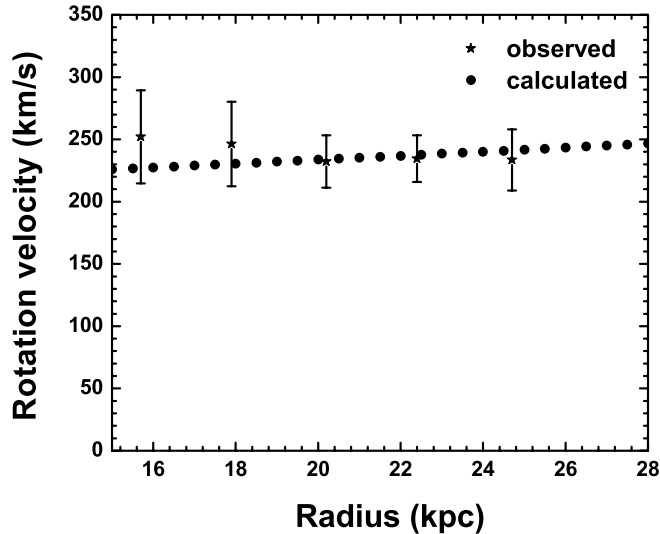


FIG. 2.—Plot of the rotation velocity (in km s^{-1}) vs. radius (in kpc) for the best-fit case of an isothermal halo of oblate shape with an axis ratio $q = 0.4$. Our model rotation curve matches well with the observed data (Widrow et al. 2003) within the error bars.

the value given by equation (10); hence, we are justified in using the above simpler form.

For the spherical bulge, the rotation velocity $v_{\text{bul}}(R)$ is given by

$$v_{\text{bul}}^2(R) = \frac{GM_{\text{bul}}(R)}{R}, \quad (11)$$

where $M_{\text{bul}}(R)$, the mass enclosed within a sphere of radius R for a Hernquist bulge, is given by the right-hand side of equation (5).

For an oblate halo of axis ratio q and density index p , the circular speed v_{halo} is obtained by differentiating the expression for the potential from Sackett & Sparke (1990) and Becquaert & Combes (1997) to be

$$v_{\text{halo}}^2(R) = 4\pi G\rho_0 q \int_0^{1/q} \frac{R^2 x^2 \{1 + R^2 x^2 / [R_c^2(1 + \epsilon^2 x^2)]\}^{-p}}{(1 + \epsilon^2 x^2)^2} dx, \quad (12)$$

where $\epsilon = (1 - q^2)^{1/2}$. We obtain the value of the integral numerically in each case. So, the total rotation velocity $v(R)$ at any galactic radius R is given by adding the contributions for the three components in quadrature as

$$v^2(R) = v_{\text{disk}}^2(R) + v_{\text{bul}}^2(R) + v_{\text{halo}}^2(R). \quad (13)$$

Next, we performed the χ^2 analysis of the calculated distributions with respect to the observed one for each of the $p = 1, 1.5$, and 2 cases. The galactic rotation curve for M31 is given by Widrow et al. (2003) and Carignan et al. (2006). We choose the rotation curve from Widrow et al. (2003) for our analysis, following Geehan et al. (2006) for reasons of internal consistency, as we have used the bulge and the stellar parameters from their mass model. We find that the calculated rotation curves do not depend significantly on the shape of the halo, i.e., q . Also, all three density indices ($p = 1, 1.5$, and 2) give a reasonably good fit to the observed rotation curve, in that they lie well within the error bars of the observed curve in the radial range of 2 – 30 kpc. However, in terms of the χ^2 analysis, $p = 1$ (the isothermal case) is the most favored.

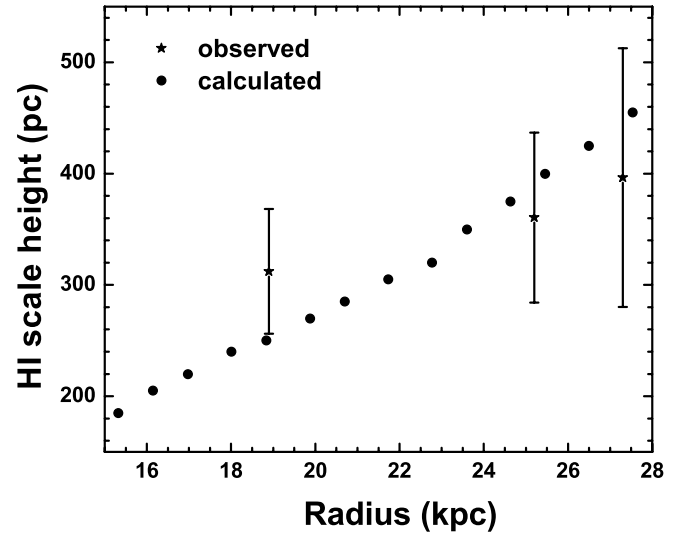


FIG. 3.—Plot of H I scale height (in pc) vs. the radius (in kpc) for the best-fit case of an isothermal halo of oblate shape with an axis ratio $q = 0.4$. The flattened halo of our best-fit model predicts a H I scale height distribution that agrees well with observations (Braun 1991) within the error bars.

4.3. The H I Scale Height Constraint

Now, for each of the above three cases ($p = 1, 1.5$, and 2), we considered only those grid points for H I scale height determination whose χ^2 values were less than 11, which is the total number of data points in the observed rotation curve. Elementary statistics suggests that a model distribution can be taken to be a reasonably good fit if its χ^2 value with respect to the observed distribution is of the order of the number of data points in the observed distribution (Bevington 1969). Also, for these given sets of grid points, we have checked that the rotation curve lies well within the error bars in the region of interest, i.e., the outer galactic region. For $p = 1$, there were 3684 such grid points, 4910 for $p = 1.5$ and 5799 for $p = 2$.

For the set of grid points chosen above, we calculated the H I scale height in the outer galactic region, i.e., beyond three disk scale lengths ($R = 16.2$ kpc), following the analysis done for the Galaxy case (Narayan et al. 2005), and obtained the χ^2 with respect to the observed scale height data (Braun 1991). The dark matter halo is expected to be more important in the outer parts, and hence, the scale height values in this range are used as a constraint to obtain the halo parameters.

4.4. Resulting Best-Fit Halo Parameters

We find that a flattened, isothermal halo ($p = 1, q = 0.4$) with a small central density ($0.011 M_{\odot} \text{ pc}^{-3}$) and a core radius of 21 kpc provides the best fit to both the observed rotation curve and the H I scale height data. The other density profiles ($p = 1.5$ and 2) give higher values for the χ^2 minimum and, hence, are not favored; however, the dependence on the power-law index p is weak. Interestingly, these also give $q = 0.4$ as the preferred shape and the same central density but with a higher core radius of 27 kpc and 34 kpc, respectively.

In Figure 2 we compare our best-fit rotation curve with the observed one in the outer regions, although the fit was done over the entire radial range of 2–30 kpc (§ 4.2). Similarly, Figure 3 depicts the best-fit scale height distribution in the outer disk region. In Figure 4 we compare the resulting scale height distributions for the various values of $q = 0.2$ – 1 in steps of 0.2, obtained using the best-fit values for ρ_0 and R_c in each case. It shows that

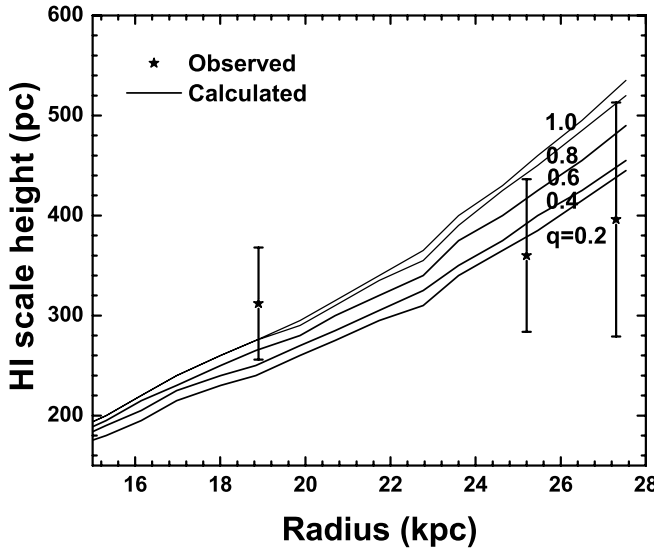


FIG. 4.—Plot of the H I scale height (in pc) vs. radius (in kpc) for an isothermal density profile and for different values of flattening: $q = 0.2, 0.4, 0.6, 0.8$, and 1 , for the best-fit values of ρ_0 and R_c in each case. This shows that a range of values between $q = 0.4$ and 0.6 gives fits to the observed data within the error bars, but the χ^2 analysis identifies $q = 0.4$ as the best-fit case.

although the χ^2 analysis selects $q = 0.4$ to be the best fit, a range of q values between 0.4 and 0.6 gives fits to the observed data within the error bars—but the departure of the calculated distribution from the real data points increases with increasing q . This is further illustrated in Figure 5, where we plot the χ^2 value for the best-fit case for each axis ratio versus the axis ratio, q . The χ^2 shows a clear minimum at $q = 0.4$, which is thus the axis ratio that best explains the observations. In particular, a flattened halo ($q = 0.4$) is clearly distinguished from and preferred over the spherical case ($q = 1$).

Interestingly, such flattened halos lie at the most oblate end of the distribution of halo shapes obtained in recent Λ CDM

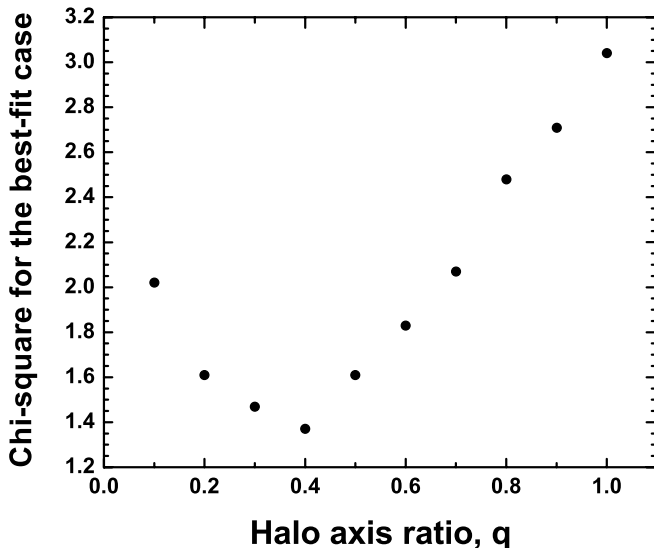


FIG. 5.—Plot of χ^2 for the best-fit case for a given axis ratio vs. the axis ratio, q , of the dark matter halo. The χ^2 shows a clear minimum at $q = 0.4$ which is thus the axis ratio that best explains the observations. Note that a flattened halo ($q = 0.4$) is clearly distinguished from and preferred over the spherical case ($q = 1$).

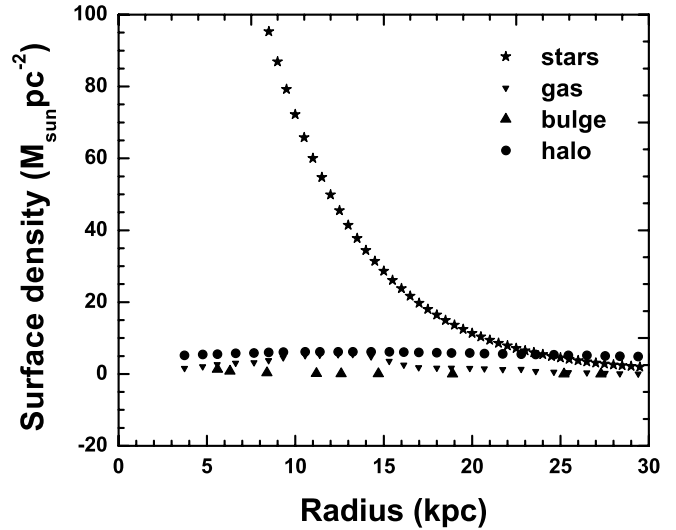


FIG. 6.—Plot of stellar, gaseous, bulge, and halo surface densities within the H I scale height in units of $M_\odot \text{ pc}^{-2}$ vs. radius in kpc. It shows that the stellar surface density is comparable to the halo surface density up to ~ 25 kpc, and only beyond this does the halo start to dominate the disk surface density as we go outward in the galaxy.

cosmological simulations (e.g., Bailin & Steinmetz 2005, see their Fig. 2; Bett et al. 2007, see their Fig. 13)—the axis ratio q used in the present paper is equal to the ratio of the semimajor axes c/a in these papers. Thus, either M31 is an unusual galaxy, or the simulations need to include additional physics, such as the effect of baryons, that could affect the shape of the halo. Further, a moderate variation in the H I gas dispersion results in a less flattened halo as shown in § 5.3.

5. DISCUSSION

5.1. H I Scale Height Data in Outer Disk

The H I scale height constraint as applied in this paper is ideally suited for application to gas-rich, late-type spiral galaxies with an extended H I disk. In order to be useful as a constraint, the H I scale height data should be available beyond $3R_d-4R_d$ and even farther out in the galaxy. This is where the disk gravitational force begins to drop out and the dark matter halo takes over. We note that obtaining the H I scale height data is an observationally challenging task (Sancisi & Allen 1979), and therein lies the main difficulty in using this method. As far as our work is concerned, the observational data (Braun 1991) gives only three data points beyond $R = 3R_d$. We consider the region only beyond $R = 3R_d$ following the Galaxy case (Narayan et al. 2005). Also, the irregularity or the scatter in the observed data in the inner region suggests the presence of a bar or spiral arm or some unknown structure and is therefore excluded from the analysis.

In Figure 6 we illustrate the above point by plotting the halo surface density within the H I scale height, as well as the corresponding values for the bulge, stars, and H I gas versus the radius. For using the H I scale height constraint, the vertical force close to the galactic midplane is needed; this is why the surface density of the halo within the H I scale height is included. This figure shows that the halo surface density just begins to take over the stellar density at the point beyond which we do not have any observed data. Availability of more data points in the outer parts, with lower error bars, is thus clearly desirable and would yield a tighter constraint on the halo shape and the density profile.

5.2. Simultaneous Constraints

The calculated rotation curve does not depend on the shape of the halo (q). All the q values give equally good fits to the observed data. Surprisingly, the χ^2 minima for the rotation curve and the H I scale height data, taken separately, lie on different regions of the grid. The best-fit to the rotation curve alone gives high values of the central density and small values of the core radius. The best-fit to the scale height data, on the other hand, gives a lower central density and a larger core radius. Geehan et al. (2006) obtained a best-fit ρ_0 of $0.033 M_\odot \text{pc}^{-3}$ (somewhat higher than the value we get) and R_c of 8.2 kpc, probably because they had used the rotation curve as the only constraint. We, on the other hand, have used two complementary constraints: the planar one involving the rotation curve and the vertical one involving the H I scale height. This allows us to uniquely determine the physical parameters of the halo and the true minimum in the grid spanning all the parameters for the dark matter halo.

We find that the observed H I scale height increases linearly with radius and does not flare. This can be explained if the halo is flattened and, consequently, implies a smaller central density, while keeping the same mass within a radius to explain the observed rotation curve.

5.3. Dependence on the H I Velocity Dispersion

The calculation of the H I scale height is crucially dependent on the chosen value of the vertical velocity dispersion of H I. We do not have any observationally measured value for the gas dispersion for M31. Here, we have assumed it to be constant at 8 km s^{-1} at all radii, as is observed for about 200 galaxies (Lewis 1984). If at all, the observed dispersion falls off with radius very gradually in the outer galaxy (Kamphuis 1993; Narayan et al. 2005). Repeating the whole analysis for a slightly smaller value of $(v_z)_{\text{H}_1} = 7 \text{ km s}^{-1}$, we find the best-fit ρ_0 and R_c to be $0.007 M_\odot \text{pc}^{-3}$ and 19.5 kpc, respectively, with $q = 0.8\text{--}0.9$, implying a less oblate halo, but with larger χ^2 values, than obtained for the best-fit case with 8 km s^{-1} in § 4.4. Physically, this trend can be explained as follows. In this case, the pressure support is smaller; hence, the gravitational force required to balance it has to be smaller to match the same observed data; hence, a less flattened halo is expected.

We also tried a case with a small radial falloff in the H I dispersion from 8 to 7 km s^{-1} in the outer disk between 18 and 27 kpc. This variation assumed is ad hoc, but it allows us to explore the effect of such a gradient on the halo shape deduced. In this case, again the best-fit is obtained for a less oblate halo of $q = 0.5\text{--}0.6$ (compared to the $q = 0.4$ obtained for a constant dispersion of 8 km s^{-1} , § 4.4). Here, χ^2 values are lower, but show a shallow minimum for the dependence on the halo shape q . This is because, in this case, the observed fairly flat scale height distribution is sought to be mainly explained by a radial variation in the gas dispersion. While this gives lower χ^2 values as expected, it also has a weak dependence on the halo shape, which is therefore not constrained well.

It is interesting that a small radial gradient in gas dispersion results in a rounder halo ($q \sim 0.6$) which is more typical of the halo shapes seen in the cosmological simulations (Bailin & Steinmetz 2005; Bett et al. 2007). This shows how crucial the value of the gas velocity is in this model in determining the flattening of the halo, which has possible implications for the galaxy formation scenarios. This highlights the necessity of accurate measurement of gas dispersion in galaxies.

5.4. Comparison with the Milky Way Galaxy

The ratio of the total mass in the halo to the total mass in the disk (in stars and gas) within a certain radius is an important physical quantity, since it tells one how significant the halo is at a certain radius. For the best-fit value for $p = 1$ and $q = 0.4$, we calculate the halo mass as a function of the radius by integrating the halo density profile as given in equation (7). The disk mass in the two components is as observed (§ 3.2). It is now known that M31 has an extended disk up to 40 kpc with a similar disk scale length in the inner and outer regions (Ibata et al. 2005). We find that the fraction of the total mass in a dark matter halo is 83% within $R = 30$ kpc or about $5R_d$ and is 89% within $R = 40$ kpc or about $7R_d$. In comparison, for the Galaxy, using the isothermal halo model for the Galaxy and the stellar disk model as given by Mera et al. (1998) and the observed values of H I and H₂ gas (Scoville & Sanders 1987), we obtain the corresponding ratio of the halo mass to the total mass to be 80% within $5R_d$ ($= 16$ kpc) and 84% within $7R_d$ ($= 22$ kpc). These are remarkably similar in the two galaxies.

On the other hand, the scale height distribution is different in the two galaxies; it is nearly flat, increasing linearly for M31, whereas it flares in the outer Galaxy. To explain this, an isothermal, flattened, oblate-shaped halo is needed for M31 as shown here, whereas using a similar approach, it was shown that a spherical halo with density falling faster than an isothermal profile is needed to explain the data for the Galaxy (Narayan et al. 2005). Thus, the dark matter halo shapes and density profiles do not appear to be universal even in large spiral galaxies.

6. CONCLUSIONS

We have used both the observed rotation curve and the outer galactic H I scale height data to constrain the dark matter halo profile of M31. We have systematically explored various shapes and power-law indices for the density distributions for the halo to fit the observed data. Our galactic disk model consists of coupled stars and H I gas, where the gas gravity is taken into account on an equal footing with the stellar gravity. We find that an oblate isothermal halo with a central density of $0.011 M_\odot \text{pc}^{-3}$ and a core radius of 21 kpc best fits the observations. The axis ratio for the best-fit result is 0.4. This is in sharp contrast to the spherical halo used to model M31 in the literature so far. The rotation curve constraint alone is usually used, which determines the mass within a radius but cannot uniquely determine the shape of the halo. The present work highlights the fact that using the two simultaneous and complementary constraints of rotation curve and the H I scale height data in the outer galactic region allows one to identify the shape as well as the density distribution of the dark matter halo in spiral galaxies.

We stress that the availability of more data points for the H I scale heights in the outer galaxy beyond 5–6 disk scale lengths and an accurate determination of the H I gas velocity dispersion would provide a tighter constraint for the shape and the density profile of the dark matter halo. In fact, having such data for other galaxies would allow the above method to be applied to a systematic study of the dark matter halo properties in different galaxies.

We thank the anonymous referee for helpful comments which greatly improved the presentation of results in the paper. We thank Shashikant Gupta for his help with optimizing the numerical code.

REFERENCES

Bailin, J., & Steinmetz, M. 2005, *ApJ*, 627, 647

Banerjee, A., & Jog, C. J. 2007, *ApJ*, 662, 335

Becquaert, J. F., & Combes, F. 1997, *A&A*, 325, 41

Begeman, K. 1987, Ph.D. thesis, Univ. Groningen

Bett, P., Eke, V., Frenk, C. S., Jenkins, A., Helly, J., & Navarro, J. 2007, *MNRAS*, 376, 215

Bevington, P. R. 1969, *Data Reduction and Error Analysis for the Physical Sciences* (New York: McGraw-Hill)

Binney, J., & Merrifield, M. 1998, *Galactic Astronomy* (Princeton: Princeton Univ. Press)

Binney, J., & Tremaine, S. 1987 (Princeton: Princeton Univ. Press)

Braun, R. 1991, *ApJ*, 372, 54

Carignan, C., Chemin, L., Huchtmeier, W. K., & Lockman, F. J. 2006, *ApJ*, 641, L109

de Zeeuw, T., & Pfenniger, D. 1988, *MNRAS*, 235, 949

Geehan, J. J., Fardal, M. A., Babul, A., & Guhathakurta, P. 2006, *MNRAS*, 366, 996

Hernquist, L. 1990, *ApJ*, 356, 359

Ibata, R., Chapman, S., Ferguson, A. M. N., Lewis, G., Irwin, M., & Tanvir, N. 2005, *ApJ*, 634, 287

Kalberla, P. M. W., Dedes, L., Kerp, J., & Haud, U. 2007, *A&A*, 469, 511

Kamphuis, J. J. 1993, Ph.D. thesis, Univ. Groningen

Kent, S. M. 1986, *AJ*, 91, 1301

—. 1987, *AJ*, 93, 816

Kerins, E., et al. 2001, *MNRAS*, 323, 13

Koper, E. 1993, Ph.D. thesis, State Univ. Leiden

Lewis, B. M. 1984, *ApJ*, 285, 453

Lewis, J. R., & Freeman, K. C. 1989, *AJ*, 97, 139

Mera, D., Chabrier, G., & Schaeffer, R. 1998, *A&A*, 330, 953

Narayan, C. A., & Jog, C. J. 2002a, *A&A*, 390, L35

—. 2002b, *A&A*, 394, 89

Narayan, C. A., Saha, K., & Jog, C. J. 2005, *A&A*, 440, 523

Navarro, J. F., Frenk, C. S., & White, S. D. M. 1996, *ApJ*, 462, 563

Olling, R. P. 1996, *AJ*, 112, 457

Olling, R. P., & Merrifield, M. R. 2000, *MNRAS*, 311, 361

—. 2001, *MNRAS*, 326, 164

Rohlf, K. 1977, *Lectures on Density Wave Theory* (Berlin: Springer)

Sackett, P. D., & Sparke, L. S. 1990, *ApJ*, 361, 408

Sancisi, R., & Allen, R. J. 1979, *A&A*, 74, 73

Scoville, N. Z., & Sanders, D. B. 1987, in *Interstellar Processes*, ed. H. A. Thronson & D. J. Hollenbach (Dordrecht: Reidel), 21

Seigar, M. S., Barth, A. J., & Bullock, J. S. 2008, *MNRAS*, in press (astro-ph/0612228)

Sofue, Y., & Kato, T. 1981, *PASJ*, 33, 449

Tamm, A., Tempel, E., & Tenjes, P. 2007, *MNRAS*, submitted (arXiv: 0707.4375v1)

Widrow, L. M., & Dubinski, J. 2005, *ApJ*, 631, 838

Widrow, L. M., Perrett, K. M., & Suyu, S. H. 2003, *ApJ*, 588, 311

Wouterloot, J. G. A., Brand, J., Burton, W. B., & Kwee, K. K. 1990, *A&A*, 230, 21